Effect of discharge voltage on capacitively coupled, parallel plate rf hydrogen plasmas

2005 Plasma Sources Sci. Technol. 14 459

(http://iopscience.iop.org/0963-0252/14/3/007)

INSTITUTE OF PHYSICS PUBLISHING PLASMA SOURCES SCIENCE AND TECHNOLOGY
Plasma Sources Sci. Technol. **14** (2005) 459–466 doi:10.1088/0963-0252/14/3/007

Effect of discharge voltage on capacitively coupled, parallel plate rf hydrogen plasmas

P Diomede, M Capitelli and S Longo

Dipartimento di Chimica dell'Universita' di Bari, Via Orabona 4, 70126 Bari, Italy
and
IMIP/CNR, Sez. Bari, Via Orabona 4, 70126 Bari, Italy

Received 21 February 2005, in final form 18 April 2005
Published 17 May 2005
Online at stacks.iop.org/PSST/14/459

Abstract
In this paper we present a parametric study of the effect of discharge voltage on capacitively coupled, parallel plate (CCPP) radio frequency discharges in pure hydrogen at low pressure, performed using a 1D(r)2D(v) particle in cell/Monte Carlo collision model with self-consistent neutral kinetics and also compare our results with experimental and theoretical ones reported in the literature. In the first part of the paper, we review the essential features of the numerical code, together with the database of plasma particles and neutral kinetics data. Results are discussed, in particular, for charged particle density and energy, the appearance of the double layer phenomenon, the plasma potential and the atom density. A possible role of photoelectric emission in the charged particle balance is also discussed.

1. Introduction

This work deals with the modelling of capacitively coupled, parallel plate (CCPP) radio frequency discharges in pure hydrogen at low pressure. There are several reasons for the attention still devoted in the literature to this kind of discharge. On the application side, hydrogen is probably the most important reactive component of gas mixtures used to feed plasma processing reactors, for example in combination with sylane or hydrocarbons, and CCPPs are still the most used devices for routine plasma processing because of their simplicity and the possibility to produce large plasma volumes. On the fundamental science side, the small molar mass and intermediate electronegativity of hydrogen make this kind of discharge plasma of interest for its peculiar phenomenology (e.g. the double layer phenomenon, the strongly condition-dependent negative ion yield) and this is especially true for the case of low pressure CCPPs, where the role played by the oscillating sheath region and the ambipolar potential in the energy pumping of electrons makes their physics still intriguing. Despite the relative wealth of high quality material in the literature, there is still work to be performed, especially in the interpretation of experimental results and the study of the effects due to the coupling of the chemical kinetics of the neutral gas chemistry with the kinetics of charged particles under conditions when the electron energy diffusion length is comparable to the characteristic dimension of the reactor: under such conditions both the uniform plasma approximation and the local equilibrium approximation cannot be applied. In the past, only a few papers have been published with a significant coverage of these issues, most of them being based on 'fluid' modelling [1–3] of the electron/ion kinetics whose application is open to question in low pressure conditions. In contrast, particle approaches, such as the well-known particle in cell/Monte Carlo collision (PIC/MCC) method avoid using strong approximations concerning the translational distribution of charged particles or the transport quantities. Very little attention has been devoted until now to the possibilities of PIC/MCC models coupled to the chemical kinetics of neutrals when applied to such controversial plasma systems, also because of the high computational cost, which is, however, offset by the simplicity of implementation and robustness of the resulting numerical codes. In the next section, the numerical technique and the database used for hydrogen are displayed, providing a basis for the following section, where the results obtained by simulating test cases extracted from the literature are described and discussed. Our results will be compared with those obtained by other authors using fluid models in the same conditions [3] when available, as well as experimental results [3–5]. This comparison allows us to check the possibilities and the limits of the present theoretical techniques, and also to distinguish the easily understandable

disagreements due to limits imposed by approximations from real open problems, which set the ground for future physical studies.

2. Numerical method

The method used is an improved version of the one presented in [6], based on coupling a 1D(r)2D(v) PIC/MCC simulation of the charged particles with the finite rate, reaction–diffusion equations for the vibrational distribution and atomic fraction. In the model, the equations of motion for the charged particles are integrated by using the leap-frog method and the electric field is calculated by solving the Poisson equation, with a space charge obtained by using a first-order particle-grid interpolation. The electron–neutral collisions are assumed to be isotropic and the momentum transfer cross section is used. The method has been updated with an extended chemical and plasma kinetics and some improvements of the ion kinetics, which are shown in [7].

The code version for hydrogen includes several reactions and plasma phase processes. We considered five particle species in the plasma phase, i.e. electrons, H_3^+, H_2^+, H^+ and H^-, and 16 neutral components, i.e. $H_2(v = 0$–$14)$ and hydrogen atoms.

In the plasma model the particle ensemble is represented by the set of numbers

$$\{i, r(i), v(i), t_c(i), s(i)\}_{i \leqslant 1 \leqslant N}; \quad N = \sum_s N_s. \tag{1}$$

Here i identifies the ith simulated particle, $r(i)$ and $v(i)$ are the position and velocity vectors assigned to the particle, $s(i)$ is the particle species and $t_c(i)$ is the time left to the next Monte Carlo collision event assigned only after a collision event by

$$t_c(i) = -\frac{1}{\alpha_{s(i),\max}} \ln \eta,$$
$$\alpha_{s,\max} = \max_{r, g<g_{\max}} g \sum_k n_{c(k)}(\boldsymbol{r}) \sigma_{k,\mathrm{tot}}(g), \tag{2}$$

where η is a random number sampled from a uniform distribution in the range $0 < \eta \leqslant 1$, g is the relative speed between the charged particle and the neutral target, $g_{\max}$ is a cut-off value for g, n_c is the number density of the cth neutral component, σ is the cross section and s is the particle species as above. Unphysical (null) events due to the fact that the collision frequency is $<\alpha_{s,\max}$ are removed by the rejection method with probability $1 - gn(\boldsymbol{r})\sigma(g)/\alpha_{\max}$.

In the calculation of this probability, the neutral velocity is randomly sampled from the thermal equilibrium distribution of gas phase particles.

Reaction processes between charged particles are also treated by the Monte Carlo method based on the time-averaged density of the partner species stored in the mesh.

The electric potential φ, in the one-dimensional gap of length d, is derived from the Poisson equation.

We solve by a Gauss–Seidel relaxation technique [6] the steady-state rate equation for the gas composition

$$-D_c \frac{\partial^2 n_c(x)}{\partial x^2} = \sum_r (\nu'_{rc} - \nu_{rc}) k_r(\langle f_e \rangle_t) \prod_{c'} n_{c'}^{\nu_{rc}}, \tag{3}$$

where f_e is the electron energy distribution function, D_c is the diffusion coefficient of the cth neutral component and k and ν are, respectively, the rate coefficient and the molecularity of the cth species in the rth elementary process in a set of N_r.

Gas–surface reactions are included by setting appropriate boundary conditions [6].

In the case of reactions including the electron as a reactant, the rate coefficient of the process must be written as (under the approximation of static neutral target)

$$k(x) = \sqrt{\frac{2}{m_e}} \int_0^\infty \varepsilon f_e(\varepsilon, x) \sigma(\varepsilon)\, \mathrm{d}\varepsilon, \tag{4}$$

where σ is the related total cross section.

The gas phase and gas/surface processes included in the code are summarized in table 1, while the set of charged–neutral-particle collision processes is presented in table 2.

Cross sections for processes (R1) and (R8) are taken from Phelps [8]; for the rate coefficients of processes (R2) and (R3) we have used the interpolation of Loureiro and Ferrera [9], while for (R4) we have used that of Gorse *et al* [10]. The electron impact processes (R5) and (R7) also lead to molecule dissociation: details are reported in table 1 and [6] and the excitation cross sections are those of [8]. The EV processes (R6) cross sections are those by Celiberto *et al* [11],

Table 1. Gas phase and gas/surface processes included in the code (see text for references).

Reaction	Code	Name
State-to-state chemistry for the gas phase		
$e + H_2(v = 0) \rightarrow e + H_2(v = 1, \ldots, 5)$	(R1a)	eV processes
$e + H_2(v = 1, \ldots, 5) \rightarrow e + H_2(v = 0)$	(R1b)	
$H_2(v) + H_2(w) \rightarrow H_2(v-1) + H_2(w+1)$	(R2)	Mono-quantum VV energy exchange
$H_2(v) + H_2 \rightarrow H_2(v-1) + H_2$	(R3a)	Mono-quantum $H_2(v)$/H_2 VT energy exchange
$H_2(v) + H_2 \rightarrow H_2(v+1) + H_2$	(R3b)	
$H_2(v) + H \rightarrow H_2(w) + H$	(R4)	Multi-quantum H/$H_2(v)$ VT energy exchange
$e + H_2 \rightarrow e + 2H$ (via $B^3\,\Sigma_u^+$, $C^3\,\Pi_u$, $A^3\,\Sigma_g^+$, $E^3\,\Sigma_u^+$)	(R5)	$H_2(X)$ dissociation through triplet states
$e + H_2(v) \rightarrow e + H_2(w)$ (via $B^1\,\Sigma_u^+$, $C^1\,\Pi_u$)	(R6)	EV processes
$e + H_2 \rightarrow e + H + H(n = 2$–$3)$	(R7)	Dissociation to excited atoms
$e + H_2 \rightarrow H + H^+ + 2e$	(R8a)	Mixed atom/ion channels
$e + H_2 \rightarrow H_2^+ + 2e$	(R8b)	
$H_2^+ + H_2 \rightarrow H_3^+ + H(\mathrm{fast})$	(R8c)	
$H_2(v > 0)$–wall $\rightarrow H_2(v = 0)$	(R9)	$H_2(v)$ deactivation on surfaces
H–wall $\rightarrow$ 1/2 H_2	(R10)	Atom recombination on surfaces
$e + H \rightarrow 2e + H^+$	(R11)	Atom ionization
$e + H_2(v = 0, \ldots, 14) \rightarrow H + H^-$	(R12)	Dissociative attachment

Table 2. Charged–neutral-particle collision processes (see text for references).

Charged/neutral particle	Collision processes
e/H_2	Elastic scattering Vibrational excitation Electronic excitation Dissociation Ionization Dissociative attachment
$e/H_2(v)$	Elastic scattering Vibrational deactivation
e/H	Elastic scattering Direct ionization
H_3^+/H_2	Elastic scattering Conversion to H^+ Conversion to H_2^+
H_2^+/H_2	Charge transfer Conversion to H_3^+
H^+/H_2	Elastic scattering
H^-/H_2	Elastic scattering Detachment
H^-/H	Detachment
H^-/H_3^+	Neutralization

from where we selected the set (v = 0–2, v' = 0–14), and we included it both in the plasma kinetics and in the chemical kinetics. The set of cross sections for dissociative attachment (R12) from level $v = 0$ to level $v = 9$, for which the reaction is endothermal, are those of [12], while for the other levels they are taken from [13]. For process (R11), cross sections are obtained from analytical calculations. The ion/neutral cross sections are after Phelps [14], except for the momentum transfer H_3^+–H_2 cross section, which is the one obtained by Simko *et al* [15]. The cross section for the total ionization of H_2 has been shared between the two channels (H_2^+, H^+) according to the branching ratios 93% and 7%, respectively [15]. The recombination rates for H^- for the reaction $H^- + H_3^+ \rightarrow 2H_2$ and associative detachment ($H^- + H \rightarrow H_2 + e$) are those given by Gorse *et al* [16].

The differential statistical weighting technique for H^+ ions already described in [6] and elaborated on further in [7] is here extended to other ions (H^- and H_2^+) in order to improve the statistics of the results. The technique is based on the introduction of 'relative weights' for particles representing different species together with statistical rejection of null events.

The particle weight of a species s, W_s, is defined as the number of real particles per simulated particle of that species. If the particle weights are different this implies that simulated particles of different species contribute different amounts to the space charge and other macroscopic quantities. A trick must be used when the particle species is changed in a collision process. For example, let us consider a mutual conversion process of a species A into a species B described by two different cross sections σ_{AB} (for A $\rightarrow$ B) and σ_{BA} (for B $\rightarrow$ A), respectively: if $W_B < W_A$, then more than one B particle must replace any A particle in conversion, and vice versa. To realize this without affecting physical quantities, one preliminarily multiplies the cross section σ_{AB} by the factor $W_A/W_B > 1$ and at any A $\rightarrow$ B collision a new particle B is produced, but A is removed only with a probability $W_B/W_A < 1$ by using the rejection method. In contrast, the cross section σ_{BA} is left unmodified and a process B $\rightarrow$ A, when occurring, is always effective to remove B, but a simulated A particle is introduced only with probability $W_B/W_A < 1$. In our case, we have assumed that the weights of H_2^+, H^+ and H^- are smaller than those of electrons and H_3^+ ions by a factor of 10. The validity of the technique can be appreciated, for example, by noting the low statistical noise on the minority H_2^+ species in the next section.

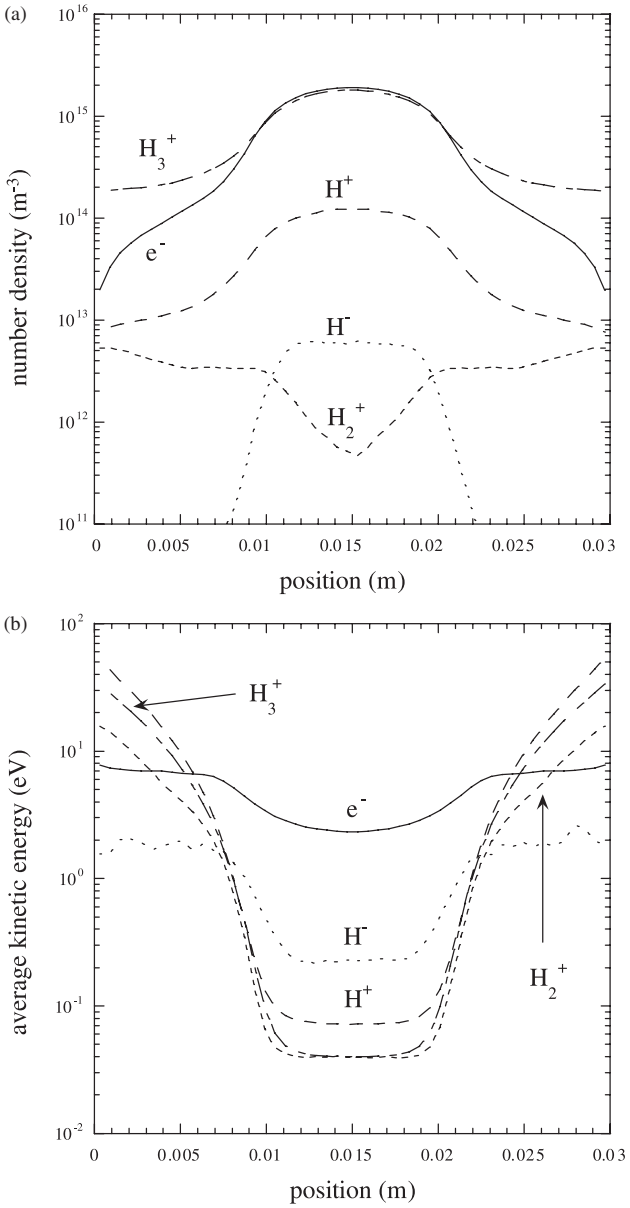

Figure 1. (*a*) Charged particle number density as a function of position for an rf voltage of 317 V ($p = 0.5$ Torr, $\nu_{rf} = 13.56$ MHz, $d = 0.03$ m, $\gamma_V = 0.02$, $\gamma_H = 0.0033$), (*b*) charged particle average kinetic energy as a function of position for an rf voltage of 317 V.

Moreover, an additional ad hoc technique has been implemented in order to speed up the convergence of the negative ion kinetics: we scale both α (the H^- production rate) and β (the loss frequency per particle) to $k\alpha$ and $k\beta$ respectively, with $k > 1$, while keeping $n(H^-) = \alpha/\beta$

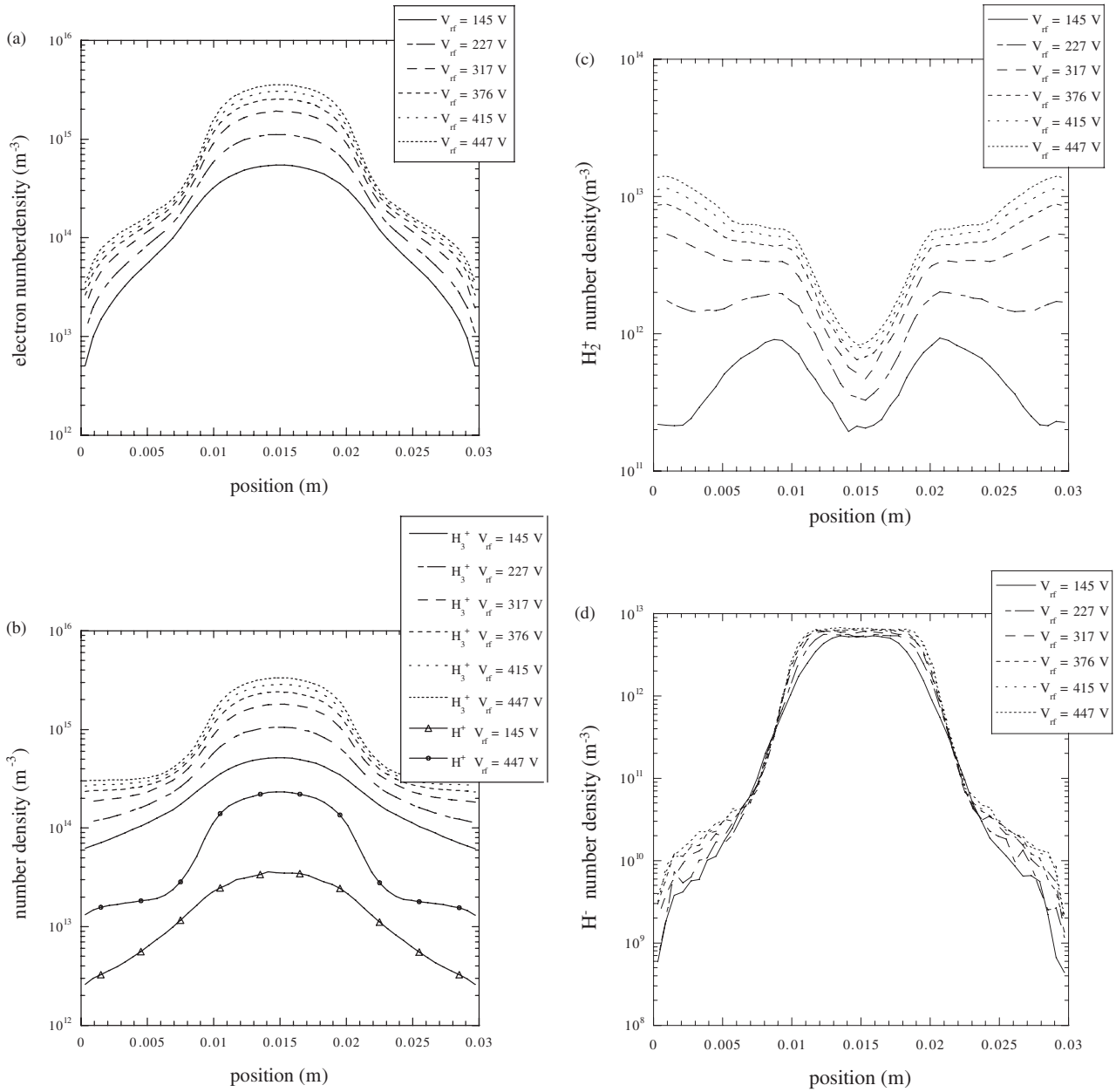

Figure 2. (*a*) Electron number density as a function of position for different values of the rf voltage considered. (*b*) H_3^+ number density as a function of position for different values of the rf voltage considered. Also shown are the values of the H^+ number density for the extreme values of the rf voltage considered. (*c*) H_2^+ number density as a function of position for different values of the rf voltage considered. (*d*) H^- number density as a function of position for different values of the rf voltage considered.

constant. This implies scaling the cross sections for attachment and detachment, and the rate coefficients in the treatment of H^- recombination. The technique works since electrons and other ion densities are not affected significantly by attachment or H^- detachment. This has been checked by direct comparison with code results with $k = 1$ [7].

3. Results and discussion

We have analysed using this model a pure hydrogen rf discharge plasma produced by the parallel-plate configuration, i.e. one plane electrode surface ($x = 0$) is kept at electric potential $V = 0$ (grounded), while the opposite one ($x = d$) is assumed to be driven by an external generator to an oscillating potential given by $V_{\rm rf} \cos 2\pi \nu_{\rm rf} t$.

The PIC part of the model works here with the total number of simulated particles in the range $(3-6) \times 10^4$, and the time step is 5×10^{-11} s, a value low enough to prevent numerical instabilities associated with electron plasma oscillations [17] but also to solve accurately the electron motion under the Courant condition. A uniform mesh of 400 cells is used to solve the Poisson equation, while a mesh of 50 cells is used to solve the reaction/diffusion equation for the neutrals.

The code was run for a physical time corresponding to several hundreds of rf cycles in order to reach a steady-state solution for the charged particle kinetics, in the sense that the

average values of transport quantities over one cycle do not change anymore with time.

In this section the influence of rf voltage on the discharge characteristics is observed. Moreover, a comparison between the results of our model and experimental results obtained by TALIF [4] (H atom density) and Langmuir probe [3] (electron density and plasma potential) measurements, varying the rf voltage, is illustrated.

The physical conditions for this test case are: discharge pressure 0.5 Torr (H atom density case) and 0.3 Torr (electron density and plasma potential case), $\nu_{rf} = 13.56$ MHz, $d = 0.03$ m, $\gamma_V = 0.02$. For the value of γ_V, the vibrational deactivation probability on the electrode surface of hydrogen molecules, a geometric average of the data found in [18–22] is used. The gas temperature is set to 300 K.

Figure 1(*a*) shows the trend of the time-averaged charged particle number density as a function of the position for an rf voltage of 317 V, which is the intermediate value used in the voltage parametrization, and a pressure of 0.5 Torr. The known phenomenology of discharge plasmas is retrieved: the plasma is neutral in the centre (bulk) region while two positive regions (the sheaths) develop in contact with the electrode surface, following the absorption of a fraction of the electrons, which move considerably faster than ions in the plasma. Also, it must be noted how negative ions accumulate in the very centre of the discharge by dropping into the self-generated ambipolar potential well.

In figure 1(*b*), the charged particle time-averaged kinetic energy as a function of position for the test case is shown: positive ions are thermalized to the gas temperature in the bulk while they reach fairly high energies in the proximity of the electrode surfaces, while negative ions, which are confined in the centre of the discharge, do not reach such high energies. Electrons, which are not effectively thermalized by collisions with the gas medium, have an energy of a few electronvolts in the bulk plasma, and reach a higher energy in the sheath region.

In figures 2(*a*)–(*d*) the charged particle number density as a function of the position for different values of the rf voltage is shown. It can be seen that the density increases with the voltage along the discharge axis for all species, except the H^- ions (figure 2(*d*)), which remain almost the same. The increase where electrons are concerned (figure 2(*a*)) is quite uniform in the discharge. From figure 2(*b*) it can be seen that the same is true for H_3^+ and H^+; for this last ion, only the curves for the extreme values of the discharge voltage are displayed, to show that the H^+ trend has the same features of the H_3^+ one, but scaled by a factor, as is also clear from figure 1(*a*). The case of H_2^+ in figure 2(*c*) is different from the case of the other positive ions: there is a strong variation of the concentration in the sheath region, due to the production of H_2^+ secondary ions by the endothermal reaction

$$H_3^+ + H_2 \rightarrow H_2^+ + 3H.$$

The kinetic energy of electrons shown in figure 3 decreases in the bulk and increases in the sheaths: this is due to the fact that, by increasing the rf voltage, the potential well that traps electrons becomes deeper, so they have enough time to cool for elastic collisions before entering the sheath region again in a random way (see figure 4).

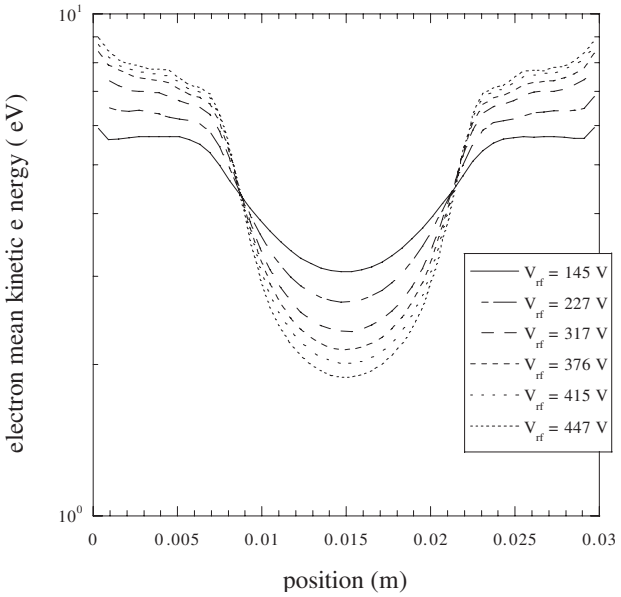

Figure 3. Electron mean kinetic energy as a function of position for different values of the rf voltage considered.

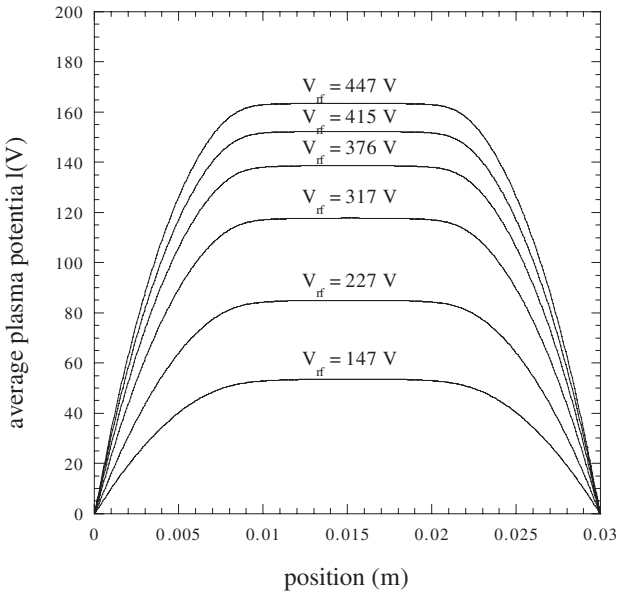

Figure 4. Average plasma potential as a function of position for different values of the rf voltage considered.

In figure 5, the variation of the kinetic energy profile for H_3^+ ions is reported: it can be seen that the increase of the discharge voltage strongly influences the energy in the sheaths, while the effect is rather null in the bulk, due to the efficient thermalization. This last result could be modified in future studies in which one accounts for the variation of the gas temperature with the deposited power. As regards the kinetic energy of the other positive ions, basically the same results are obtained, so the corresponding plots are not reported.

Figure 6 shows the variation of the kinetic energy of H^- ions and one can observe that they heat sensibly in the plasma centre by increasing the discharge voltage. This result can be interesting for the production of negative ions in this kind of discharge (see also [23]).

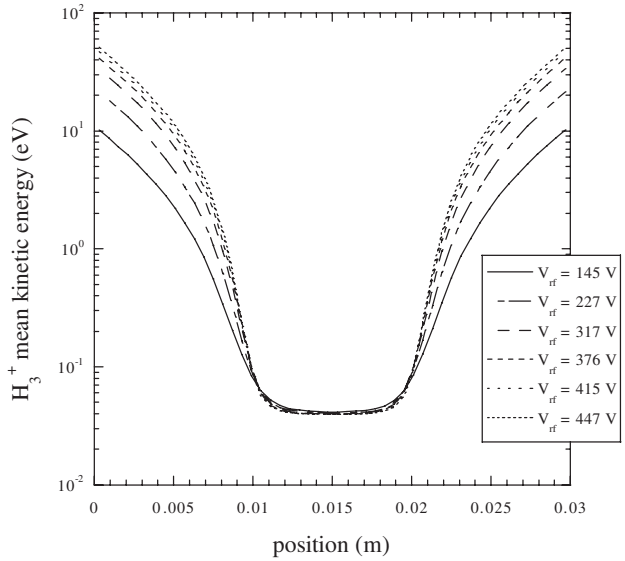

Figure 5. H_3^+ mean kinetic energy as a function of position for different values of the rf voltage considered.

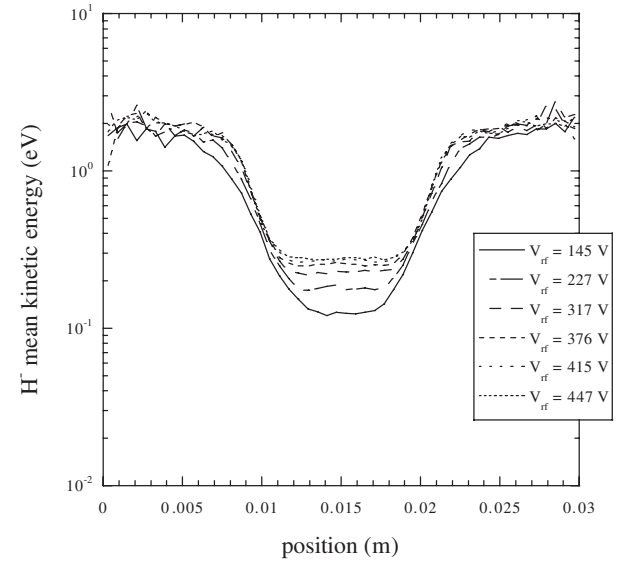

Figure 6. H^- mean kinetic energy as a function of position for different values of the rf voltage considered.

Figure 7 shows the comparison between the measured [4] and calculated H atom density, for different values of the rf voltage and for two different values of the atom recombination probability: the value $\gamma_H = 0.01$ is measured experimentally [4] using time-resolved TALIF measurements, while the value $\gamma_H = 0.0033$ is used to have a better agreement with the experimental results. It can be seen that the trend of the experimental curve is reproduced even with the first value of the recombination probability. This change of the γ_H value to fit the H atom concentration is somewhat higher than allowed by experimental errors declared by the authors of [4] on similar measurements; however, several authors in the past years found a wide range of variation of this parameter with experimental conditions and material surface properties, even for the same metal. At the same time, the agreement of the trend together with the disagreement on the absolute value is

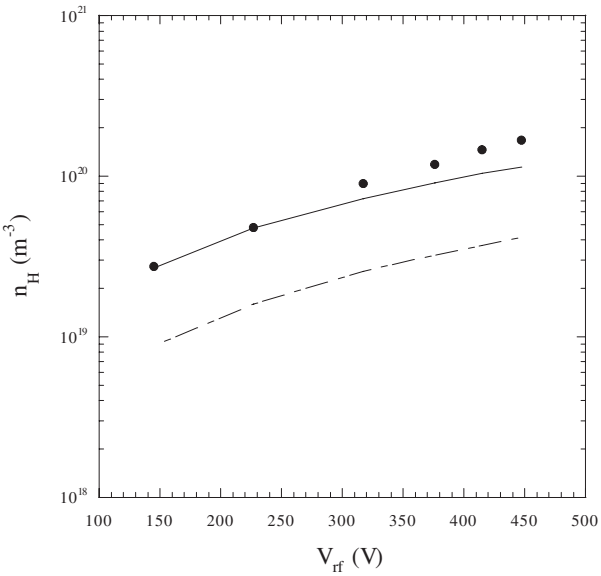

Figure 7. Hydrogen atom density versus rf voltage: comparison between measured [4] (full circles) and calculated values for atom recombination probabilities of 0.01 (— · —) and 0.0033 (——).

probably associated with features similar to those found for the electron density (figure 9), explained later.

A further comparison with experimental results has been devoted to the phenomenon of the double layer, which has been experimentally observed in radio frequency discharges in many electronegative gases, including hydrogen. This phenomenon manifests itself as a double maximum in the space profile of the emission spectrum of the plasma in selected electronic lines and close to the electrodes. This has been explained as a result of the accumulation of negative ions in the bulk plasma, which blocks the motion of the electrons towards the momentary anode. Accumulated electrons produce the secondary peak in the ionization and excitation rates when the sheath region expands again in the cathodic stage. We have applied our model to the experimental conditions of double layer formation in [5], which are those of the test case under discussion. In particular figure 8(*a*) shows a comparison of the H_α emission profile with the calculated space profile of the excitation rates of H($n = 3$) for different rf voltages, while figure 8(*b*) reports an analogous comparison for the emission and excitation rates of the $d\,^3\Pi_u$ electronic state of the hydrogen molecule. The comparison is only qualitative for the following reasons: first, the experimental discharge is asymmetric and it develops a bias voltage, second, the value of the voltage is not known for the case reported, third, at the present stage, our model does not include a kinetics of electronic states leading to the observed radiation. In any case, it is satisfactory that our model actually predicts the appearance of a double layer in hydrogen, which starts at a definite discharge condition, as in the experiment.

In figures 9 and 10 we show a comparison between our PIC code results and the experimental results in [3] for the electron density and plasma potential in the discharge centre for different values of the applied rf voltage under the same conditions of the test case in the previous figures, except for the pressure that is set to 0.3 Torr; the value assumed for γ_H is 0.0033. The model reproduces well the trend of the electron density as a function of the rf voltage, while it underestimates

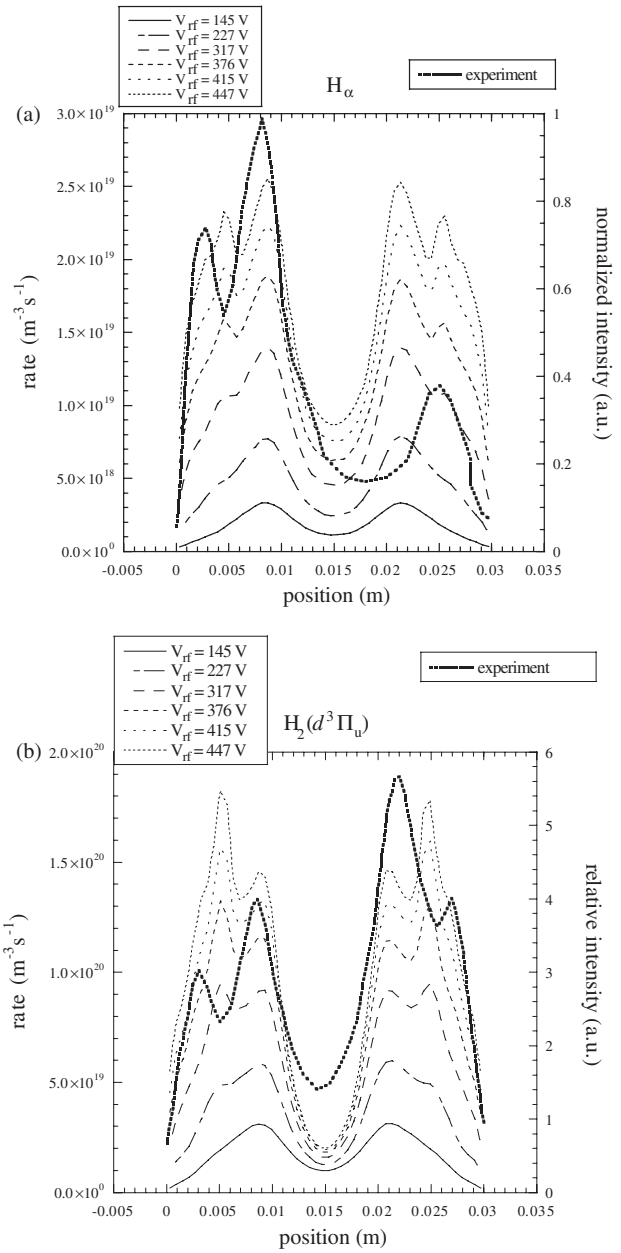

Figure 8. (*a*) Comparison of the H_α experimental emission profile [5] with the calculated space profile of the excitation rate of $H(n = 3)$ for different rf voltages. (*b*) Comparison of the experimental emission profile [5] with the calculated space profile of the excitation rate of the $d^3\Pi_u$ electronic state of the hydrogen molecule for different rf voltages.

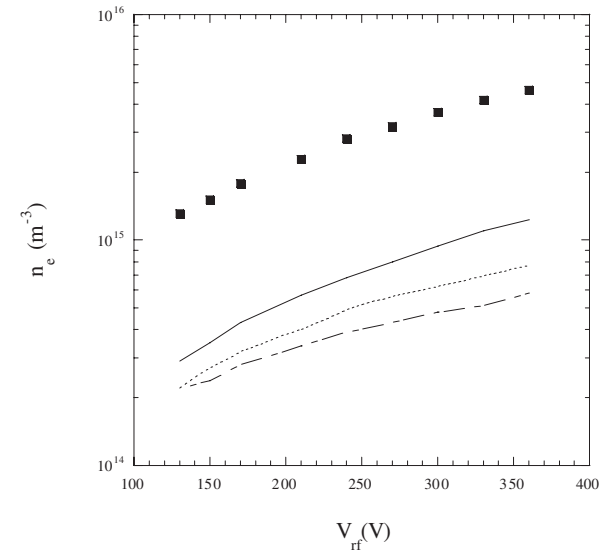

Figure 9. Electron density versus rf voltage: comparison between measured [3] (full squares) and calculated results ($p = 0.3$ Torr, $\nu_{rf} = 13.56$ MHz, $d = 0.03$ m, $\gamma_V = 0.02$, $\gamma_H = 0.0033$) of the PIC model without (——) and with (— · —) consideration of the bias voltage and the results of the model of [3] (· · · · · ·).

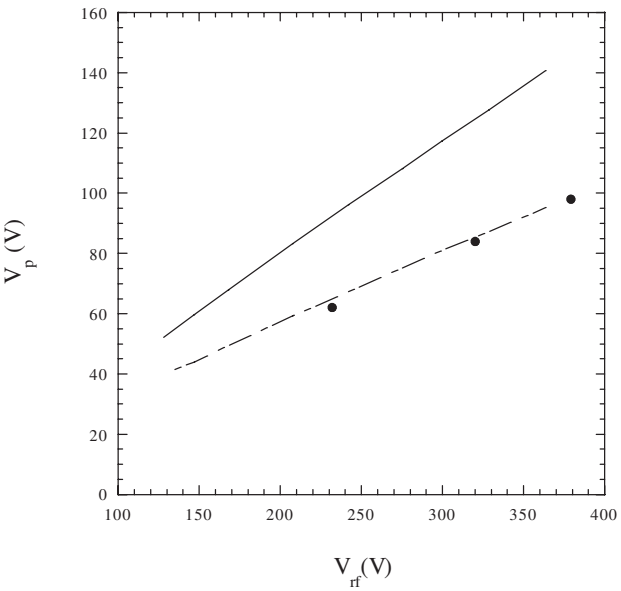

Figure 10. Plasma potential versus rf voltage: comparison between measured [3] (full circles) and calculated values for the test case without (——) and with (— · —) consideration of the bias voltage.

the values. This underestimation is also obtained with the fluid model used in [3] but there it is attributed to the incomplete description of the discharge space-charge sheaths and the simplified hydrogen kinetics considered, but this is not the case of our model. It must be noticed that the experimental reactor develops a self-bias voltage, so we also performed simulations by inserting the measured values of the bias voltage as a function of the discharge voltage, but this increases the underestimation. As regards the plasma potential, however, the model results with the bias voltage are in very good agreement with the experiment.

The good comparison of our results with those obtained by the model in [3] using a two-dimensional fluid model shows that, contrary to common wisdom, neither the dimensionality nor the fully kinetic character of the model are critical issues for the determination of the electron density in this test case. The disagreement of both codes with experimental results for the electron density is therefore a kind of open problem, asking for new ionization channels (bulk channels, e.g. ionization of metastable electronic states as well as surface ones) to be included in future codes.

As an attempt at this kind of improvement, in figure 11 there is a comparison between the experimental results for

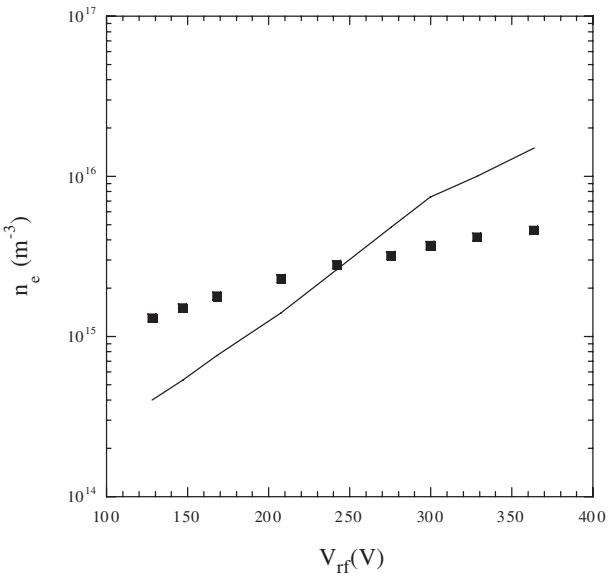

Figure 11. Electron density versus rf voltage: comparison between measured [3] (full squares) and calculated results considering the bias voltage, and a photoemission coefficient of 0.2 (——).

the electron density as a function of the rf voltage and the model results for this test case, including the bias voltage and considering an electrode photoemission mechanism with a probability equal to 0.2. For simplicity, only the EV processes were considered as a production process for photons generating the photoelectric effect on the electrodes, since in this case the radiative decay gives rise to radiation in the UV range with an energy greater than 4 eV, the typical work function value for metals. It can be seen that, in this case, the trend of the experimental results is not reproduced, while the values obtained with the model cross the experimental ones for the intermediate voltage value.

Another possible improvement of the code, which could lead to better results for the electron density, concerns an enrichment of the majority ion (H_3^+) kinetics based on future improved cross sections and inclusion of more ion/molecule processes.

4. Concluding remarks

In this paper, the effect of voltage amplitude on the CCPP/rf discharge plasma in pure hydrogen has been studied theoretically using a fully kinetic 1D(r)2D(v) PIC/MC model for five charged components coupled to the finite rate chemistry of neutral components. Results show interesting features deserving future investigations, such as the variation of the density profile of H_2^+ and H^- and the bulk energy of H^- ions, and the modulation of the double layer effect. This study is also useful for applications in view of the ubiquity of hydrogen as a component in plasma processing gas mixtures and the use of pure hydrogen plasmas in negative ion production. The comparison with experimental results is fairly good and the general picture emerging from the comparison and from the analysis of the theoretical results is encouraging as a whole, showing the good potentiality of a particle method of reduced dimensionality, very robust and of reasonable computational cost, in the study of the effects and interpretations of parameter changes in real CCPP/rf hydrogen discharges.

Acknowledgments

This work was partially supported by MIUR (Project No 2003037912_010) and ASI (Project No I/R/055/02). The calculations were performed in the framework of the GRID-FIRB project.

References

[1] Novikova T, Kalache B, Bulkin P, Hassouni K, Morscheidt W and Roca i Cabarrocas P 2003 *J. Appl. Phys.* **93** 3198
[2] Boeuf J P and Pitchford L C 1995 SIGLO-RF, PC version 1.0, a 1D User-Friendly Model for RF Discharges Simulation (Kinema Software, siglo@kinema.com, http://www.siglo-kinema.com/siglo-rf.htm, Monument, CO)
[3] Salabas A, Marques L, Jolly J, Gousset G and Alves L L 2004 *J. Appl. Phys.* **95** 4605
[4] Jolly J, Dine S and Booth J-P 2004 *Proc. 17th European Conf. on Atomic and Molecular Physics of Ionized Gases (Constanta, Romania, 1–5 September 2004)* ed V Ciupina, G Musa and R Vladoiu pp 195–6
[5] Leroy O, Stratil P, Perrin J, Jolly J and Belenguer P 1995 *J. Phys. D: Appl. Phys.* **28** 500–7
[6] Longo S and Boyd I D 1998 *Chem. Phys.* **238** 445
[7] Longo S, Capitelli M and Diomede P 2004 *Lecture Notes Comput. Sci.* **3039** 580
[8] Phelps A V 2005 Directory FTP collision_data in jila.colorado.edu
[9] Loureiro J and Ferrera C M 1989 *J. Phys. D: Appl. Phys.* **22** 1680
[10] Gorse C, Capitelli M, Bacal M, Bretagne J and Laganà A 1987 *Chem. Phys.* **11** 117
[11] Celiberto R, Janev R K, Laricchiuta A, Capitelli M, Wadehra J M and Atems D E 2001 *At. Data Nucl. Data Tables* **77** 161
[12] Capitelli M, Celiberto R and Cacciatore M 1994 *Adv. At. Mol. Opt. Phys.* **30** 321
[13] Fabrikant I I, Wadhera J M and Xu Y 2002 *Phys. Scr.* **T96** 45–51
[14] Phelps A V 1990 *J. Phys. Chem. Ref. Data* **19** 653
[15] Simko T, Martisovits V, Bretagne J and Gousset G 1997 *Phys. Rev.* E **56** 5908
[16] Gorse C, Celiberto R, Cacciatore M, Laganà A and Capitelli M 1992 *Chem. Phys.* **161** 211
[17] Skullerund H R 1968 *J. Phys. D: Appl. Phys.* **1** 1567
[18] Karo A M, Hiskes J R and Hardy R J 1985 *J. Vac. Sci. Technol.* A **3** 1222
[19] Orkin V L, Fedotov V G and Chaikin A M 1977 *Kinetics Catalysis* **18** 55
[20] Kae-Nune P, Perrin J, Jolly J and Guillon J 1996 *Surf. Sci.* **360** L495
[21] Gorse C, Capitelli M, Bretagne J and Bacal M 1985 *Chem. Phys.* **93** 1
[22] Wood B J and Wise H 1961 *J. Phys. Chem.* **65** 1976
[23] Diomede P, Longo S and Capitelli M 2005 *Eur. Phys. J.* D **33** 243